Comprehensive Evaluation Of Attitude and Orbit Estimation Using Real Earth Magnetic Field Data

Julie Deutschmann
National Aeronautics and Space Administration
Flight Dynamics Division/Code 552
Goddard Space Flight Center
Greenbelt, Maryland 20771 USA
email: julie.deutschmann@gsfc.nasa.gov
telephone: 301-286-9033
fax: 301-344-8909

Itzhack Bar-Itzhack
Sophie and William Shamban Professor of Aerospace Engineering
Faculty of Aerospace Engineering
Technion-Israel Institute of Technology
Haifa 32000 Israel
email: ibaritz@techunix.technion.ac.il
telephone:972-4-829-3196
fax: 972-4-823-1848

Abstract. A single, augmented Extended Kalman Filter (EKF) which simultaneously and autonomously estimates spacecraft attitude and orbit has been developed and successfully tested with both simulated and real magnetometer and rate data. Since the earth's magnetic field is a function of time and position, and since time is known quite precisely, the differences between the computed and measured magnetic field components, as measured by the magnetometers throughout the entire spacecraft orbit, are a function of both orbit and attitude errors. Therefore, these differences can be used to estimate both orbit and attitude. The results of testing the EKF with real magnetometer and gyro data from four satellites supported by the NASA Goddard Space Flight Center (GSFC) Flight Dynamics Division (FDD) are presented and evaluated.

Introduction

In this work, we summarize the derivation of the EKF, highlighting the development of the measurement matrix, the crucial element in combining the dependence of the magnetic field residuals on both attitude and trajectory estimation errors. The dynamics of both the attitude and trajectory errors are also presented. Magnetometer and gyro measurements from the Compton Gamma Ray Observatory (CGRO), Rossi X-Ray Timing Explorer (RXTE), the Earth Radiation Budget Satellite (ERBS), and the Total Ozone Mapping Spectrometer-Explorer Platform (TOMS-EP) are processed by the EKF. The satellites vary in inclination (23 degrees for CGRO to 97 degrees for TOMS-EP) and in size of the magnetometer quantization error (0.3 to 6.4 milliGauss). Comparisons are made with very accurate operational estimates (position, velocity, and attitude) computed at the NASA Goddard Space Flight Center (GSFC) Flight Dynamics Division (FDD). These comparisons are presented in the paper.

Both attitude and trajectory have been successfully estimated using simulated magnetometer data and rate data[1]. Large initial errors were applied with a resulting accuracy of 4 km root sum square (RSS) in position and less than 1 degree RSS in attitude. In this work, we continue the testing of the EKF with real data from the four satellites given above . The ability of the filter to overcome large initial errors and a comparison of the final accuracy achieved with each satellite is presented.

The magnetometer, due to its reliability and low cost, has been the focus of many studies in the recent past. Emphasis has been placed on using the magnetometer alone, without any additional input, to estimate the spacecraft trajectory [2, 3, 4] and attitude[5,6]. Studies have also been performed to determine the

ultimate accuracy of the magnetometer in estimating attitude when accurate rate information is available[7]. Many future low-budget missions, such as the NASA Small and Mid-Size Explorer Series and university class explorers, are looking for low cost and autonomous approaches to orbit and attitude estimation. This work could prove valuable to these missions as a prime trajectory and attitude estimation system, with coarse accuracy requirements, or as a backup to a prime system where more stringent accuracy is required. To reduce the cost, a technique for determining the spacecraft rates must be incorporated, therefore eliminating the need for an expensive gyro.

Extended Kalman Filter (EKF) Algorithm

The EKF algorithm is based on the following assumed models:

System Model:

$$\dot{\underline{X}} = \underline{f}(\underline{X}(t), t) + \underline{w}(t) \qquad (1)$$

Measurement Model:

$$\underline{y}_k = \underline{h}_k(\underline{X}(t_k)) + \underline{v}_k \qquad (2)$$

where $\underline{w}(t)$ is a zero mean white process noise, $\underline{v}_k$ is a zero mean white sequence measurement error, and $\underline{X}(t)$ is the state vector defined as

$$\underline{X}^T = [a, e, i, \Omega, \omega, \theta, C_d, \underline{q}]$$

The first six elements of $\underline{X}(t)$ are the classical Keplerian elements which determine the spacecraft position and velocity, namely, the semi-major axis (a), eccentricity (e), inclination (i), right ascension of the ascending node (Ω), argument of perigee (ω), and true anomaly (θ). C_d is the drag coefficient and $\underline{q}$ represents the attitude quaternion. The EKF consists of the measurement update stage and the propagation stage. They are described next.

EKF Measurement Update

The measurement update of the state estimate and of the estimation error covariance are performed, respectively, as

$$\hat{\underline{X}}_k(+) = \hat{\underline{X}}_k(-) + K_k[\underline{y}_k - \underline{h}_k(\hat{\underline{X}}_k(-))] \qquad (3)$$

$$P_k(+) = [I - K_kH_k]P_k(-)[I - K_kH_k]^T + K_kR_kK_k^T \qquad (4)$$

where K_k is the Kalman gain computed according to

$$K_k = P_k(-)H_k^T[H_kP_k(-)H_k^T + R_k]^{-1} \qquad (5)$$

where $H_k = H_k = \left.\frac{\partial \underline{h}_k(\underline{X}_k(t_k))}{\partial \underline{X}_k}\right|_{\underline{X}_k=\hat{\underline{X}}_k}$

P_k = estimation error covariance matrix
R_k = covariance matrix of the white sequence $\underline{v}_k$

The effective measurement used by the filter is given as

$$\underline{z}_k = \underline{B}_{m,k} - \underline{B}(\hat{\underline{X}}_k, t_k) \qquad (6)$$

where
$\underline{B}_{m,k}$ = the magnetic field vector measured by the magnetometer

$\underline{B}(\hat{\underline{X}}_k, t_k)$ = the estimated magnetic field vector as a function of the estimated state at time t_k computed using a 10^{th} order International Geomagnetic Reference Field model

While the traditional EKF algorithm updates the state estimate according to (3), we use $\underline{z}_k$ (as computed in (6)) to update the state estimate as

$$\hat{\underline{X}}_k(+) = \hat{\underline{X}}_k(-) + \hat{\underline{x}}(t_k) \qquad (7)$$

where: $\hat{\underline{x}}(t_k) = K_k\underline{z}_k$

The resulting algorithm is equivalent to the traditional EKF algorithm. A linear relationship exists between $\underline{y}_k - \underline{h}_k(\underline{X}_k(-))$ and $\hat{\underline{x}}(t_k)$, which is linearly related to the effective measurement $\underline{z}_k$. This relationship is given in Appendix A. Resulting from this linear relationship is the measurement matrix H_k, the key component in the simultaneous estimation of the position and attitude.

As seen in the derivation in Appendix A, the effective measurement can be written as

$$\underline{z}_k = H_k \underline{x}_k + \underline{v}_k \quad (8)$$

where $\underline{x}_k$ = [a, e, i, Ω, ω, θ, C_d, $\underline{\alpha}$]
$\underline{\alpha}$ = vector of three small Euler angles describing the attitude difference between the true and estimated attitudes

The EKF estimates $\hat{\underline{x}}(t_k)$ and then, for the orbital states, adds the estimate $\hat{\underline{x}}(t_k)$ to $\hat{\underline{X}}_k(-)$, the best a-priori estimate of $X(t_k)$, as shown in (7). For the attitude states, the three small angles in the vector, $\underline{\alpha}$, are used to construct dq[8]

$$dq^T = [\tfrac{1}{2}\phi \ \tfrac{1}{2}\varphi \ \tfrac{1}{2}\psi \ 1] \quad (9)$$

The attitude quaternion is then updated as

$$q_{k+1}=q_{k+1}(-)\otimes dq^{-1} \quad (10)$$

where ⊗ denotes a quaternion product.

EKF Propagation

The propagation of the state estimate, based on equation (1), is performed as

$$\dot{\hat{X}}(t)=f(\hat{\underline{X}}(t),t) \quad (11)$$

The updated estimate of the state vector, $\hat{\underline{X}}_k(+)$ is propagated from time t_k to t_{k+1} by a numerical solution of the continuous dynamics equation given in (11). The orbital dynamics are non-linear and describe a central force including both J_2 effects and drag[9]. The differential equation which governs the propagation of the quaternion is linear and requires the spacecraft rate[10]. In this work the rate is supplied by gyroscopes. The detailed dynamics equations for each state element are given in Appendix B.

The propagation of the covariance is given as

$$P_{k+1}(-)=A_k(\hat{\underline{X}}_k(+))P_k(+)A_k^T(\hat{\underline{X}}_k(+))+Q_k \quad (12)$$

where Q_k is the spectral density matrix of $\underline{w}(t)$ and A_k is the approximated transition matrix. A_k is computed using the following first order Taylor series expansion

$$A_k=I+F\Delta T \quad (13)$$

where ΔT is the time interval between gyro measurements. The Jacobian F is given as

$$F=\left.\frac{\partial f(\underline{X}(t),t)}{\partial \underline{X}}\right|_{\underline{X}=\hat{\underline{X}}} \quad (14)$$

The actual computation of F is based on the dynamics equations given in Appendix B, without J_2 effects.

Results

The four satellites, CGRO, RXTE, ERBS, and TOMS, varied in altitude, inclination, resolution of the magnetometer data in telemetry (quantization error), and frequency at which the magnetometer telemetry was received. Table I summarizes these variations.

Table I. Satellite Information

Satellite	h (km)	i (deg)	size (mG)	ΔT (sec)
CGRO	340	28.5	0.3	3-4
RXTE	580	23.0	0.3	2
ERBS	613	57	6.4	16
TOMS	483	97	4	33-34

where h = altitude
i = inclination
size = resolution of telemetry
ΔT = time between magnetometer meas.

In addition, the accuracy of the gyroscopes varied. The CGRO and RXTE gyros were considerably more accurate than those of TOMS and ERBS.

The initial errors applied to each satellite are given below in Table II. The errors displayed are the RSS errors. The errors are determined by comparing the filter position, velocity, and attitude with accurate position, velocity, and attitude estimates computed at the NASA GSFC FDD.

Table II. Initial RSS Errors

Satellite	Position (km)	Velocity (km/sec)	Attitude (deg)
RXTE	2617	2.6	15.7
ERBS	1000	1.1	11.4
CGRO	1098	1.1	12.9
TOMS	2389	2.6	13

The figures below show the position and attitude error for each satellite. Figures 1 through 3 show the RXTE RSS position error (full scale and expanded vertical axis) and RSS attitude error with an expanded vertical axis. Figures 4 through 6 show ERBS position and attitude, Figures 7 through 9 show CGRO results, and Figures 10 through 12 show the TOMS results. The velocity errors are not shown, but for each satellite they have a shape similar to the position error. Table III, preceding the figures, summarizes the final, average RSS errors for position, velocity, and attitude for each satellite.

For CGRO, ERBS, and TOMS the final position errors are comparable, with averages of 20 to 30 km. All three also converge quickly, the position estimates are under 40 km within 1 orbit, including TOMS which started with a 2389 km position error. CGRO shows the smallest oscillations overall. The position estimates from all three appear to still be converging. The data spans are limited for these three satellites so long term steady state behavior could not be studied.

CGRO has the lowest attitude error. The final average RSS attitude error is 0.2 deg. The CGRO data was extensively calibrated, the magnetometer quantization error is small and the measurement frequency, particularly of the gyro data is very high. Surprisingly, the TOMS attitude errors are also relatively small, with a final average of 0.75 degrees. This is a result of the high inclination for TOMS which results in good observability, despite the large quantization error , the low measurement frequency, and uncalibrated magnetometer data. ERBS has the highest attitude error, the final average is 1.4 deg. ERBS has the largest quantization error and also a low measurement frequency.

RXTE took considerably longer to converge, and both the attitude and position error results show a divergence in the middle of the span. RXTE underwent three attitude maneuvers during this span which perhaps lead to a deviation in the drag coefficient, which then leads to the increased errors. Once the drag coefficient converges again, the position results improve and for the last 3 orbits are very good with an average RSS position error of approximately 15 km. The final average RSS attitude errors are approximately 1 degree. The RXTE data was not calibrated at all and contains unknown disturbances which contribute to the larger final attitude error.

Table III. Final, Average, RSS Errors

Satellite	Position (km)	Velocity (km/sec)	Attitude (deg)
RXTE*	15	0.015	1.0
ERBS	25	0.03	1.4
CGRO	20	0.02	0.2
TOMS	20	0.025	0.75

*Averages are for the last 3 orbits

Conclusions

Magnetometer data and gyro data from four satellites were processed by the EKF. All four converged to final averages of 15 - 30 km in position, 0.015 - 0.03 km/sec in velocity, and 0.2 - 1.5 degrees in attitude (all RSS). Additional results also indicated that the EKF could converge from extremely large initial position and velocity errors; CGRO and TOMS overcame initial position errors exceeding 5000 km.

The data from each of the satellites differed in quantization error and measurement frequency, and the satellites were at 4 different inclinations. The higher inclinations for ERBS and TOMS resulted in quick convergence, and for TOMS gave good final results despite inaccuracies in the data and a large time between measurements. The coarse quantization of the ERBS telemetry and the infrequency of the measurements results in the lowest accuracy. The extensive calibration of the CGRO data, the small quantization errors, and the high data frequency perhaps contributed to the quick

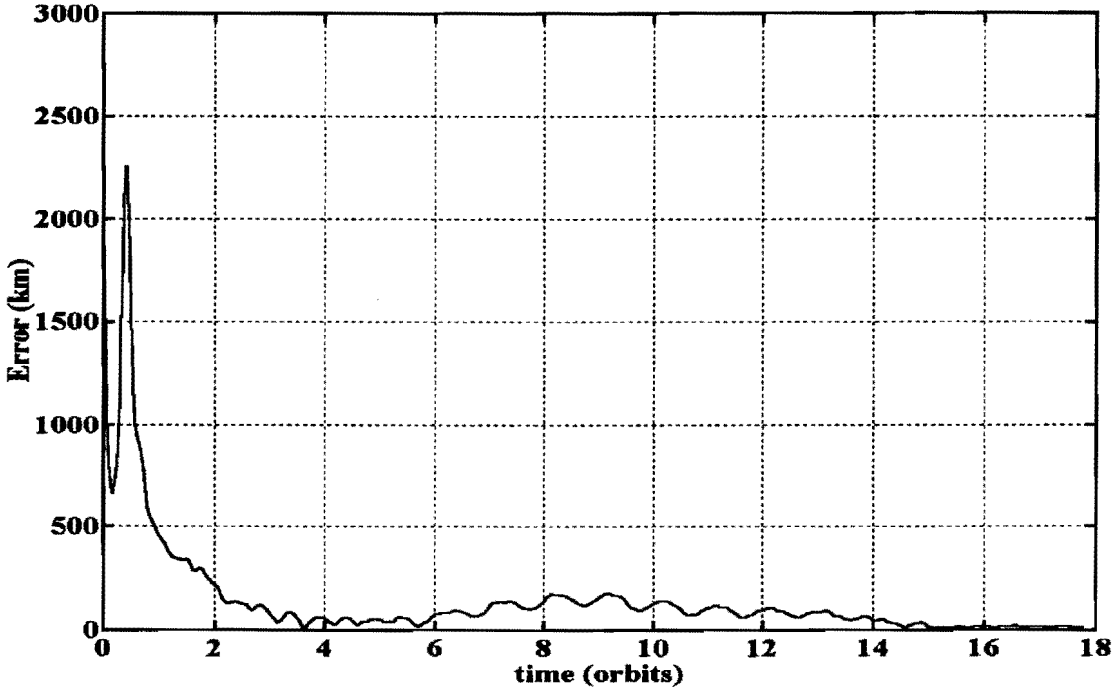

Figure 1. RXTE RSS Position Error

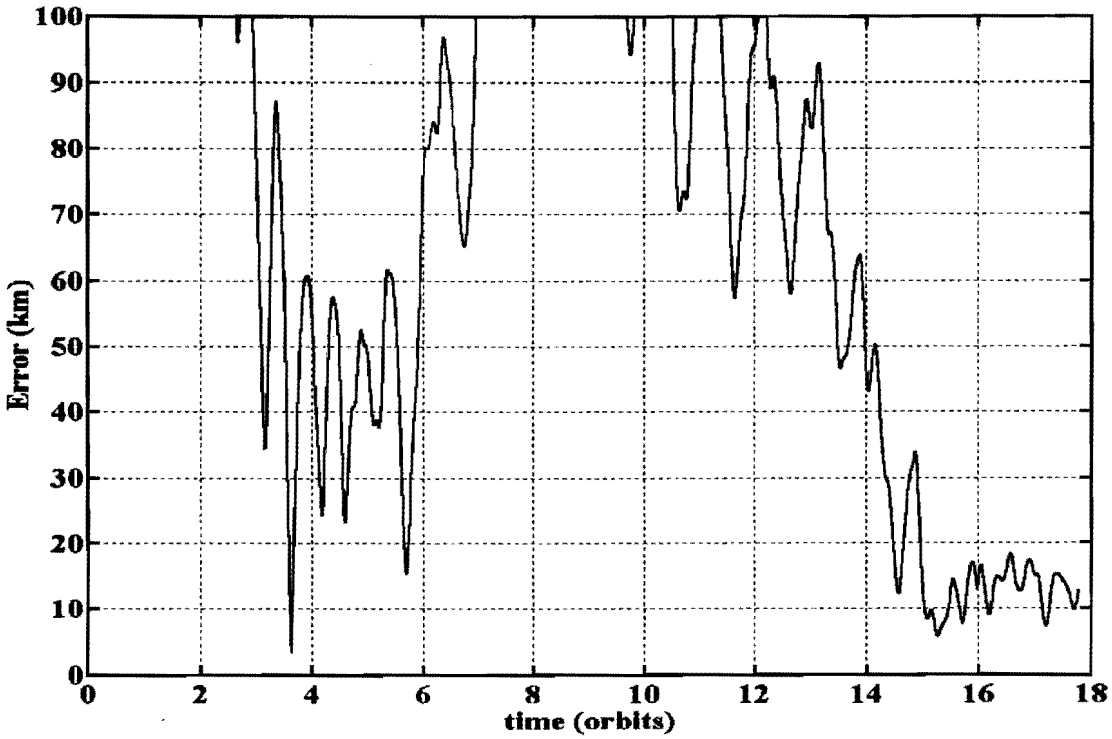

Figure 2. RXTE RSS Position Error, Expanded Axis

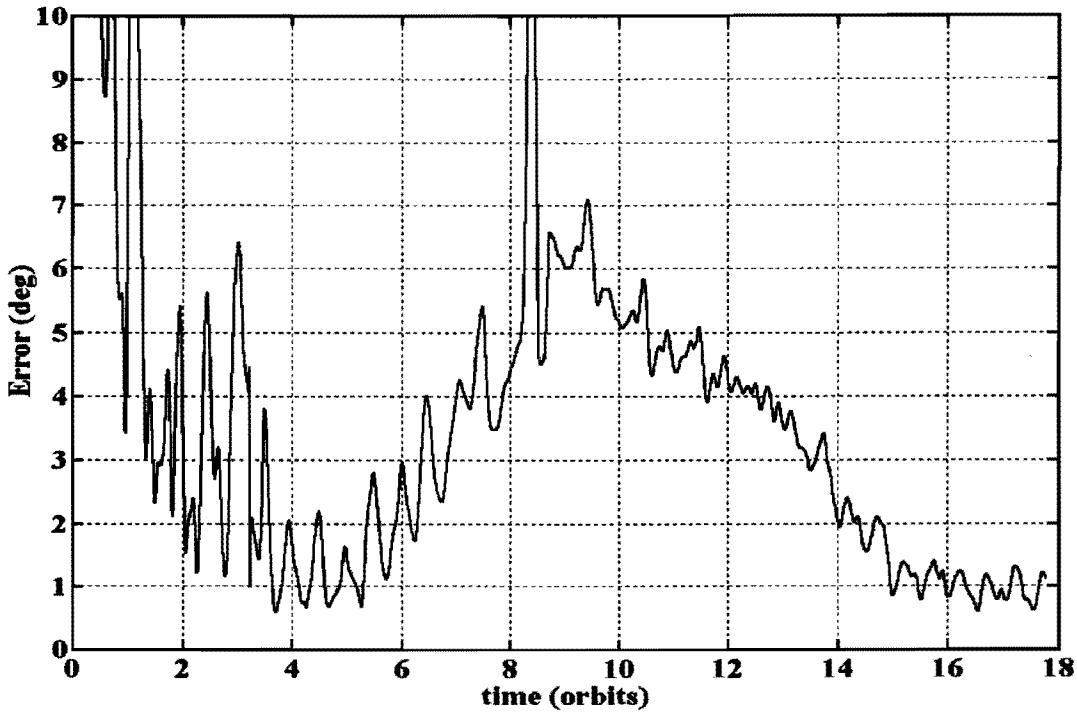

Figure 3. RXTE RSS Attitude Error, Expanded Vertical Axis

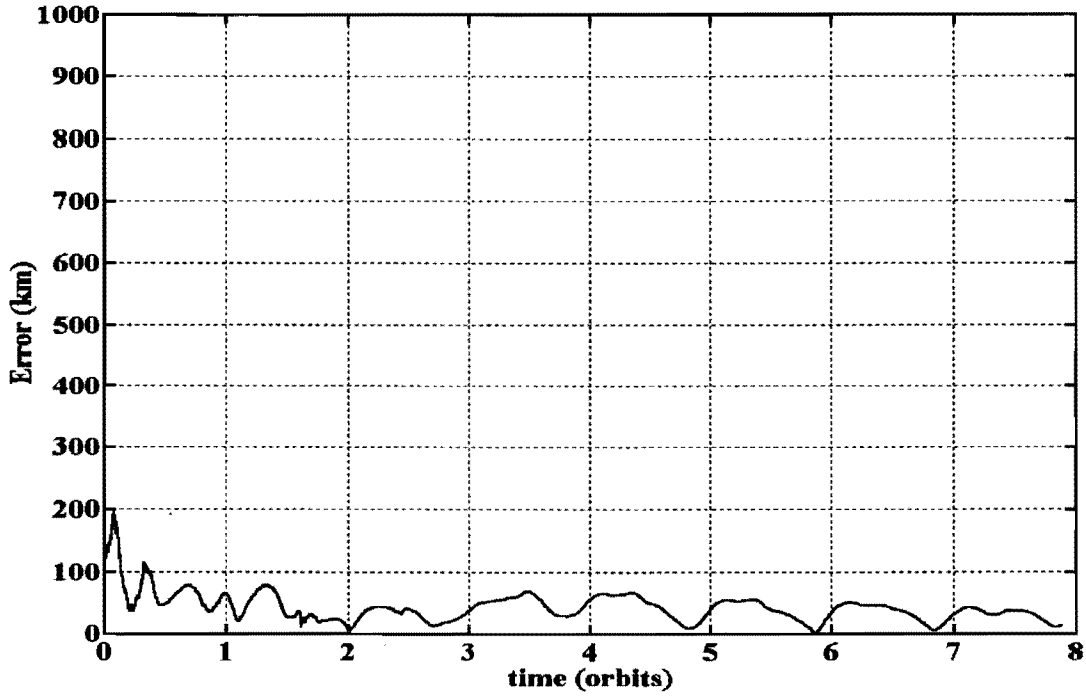

Figure 4. ERBS RSS Position Error

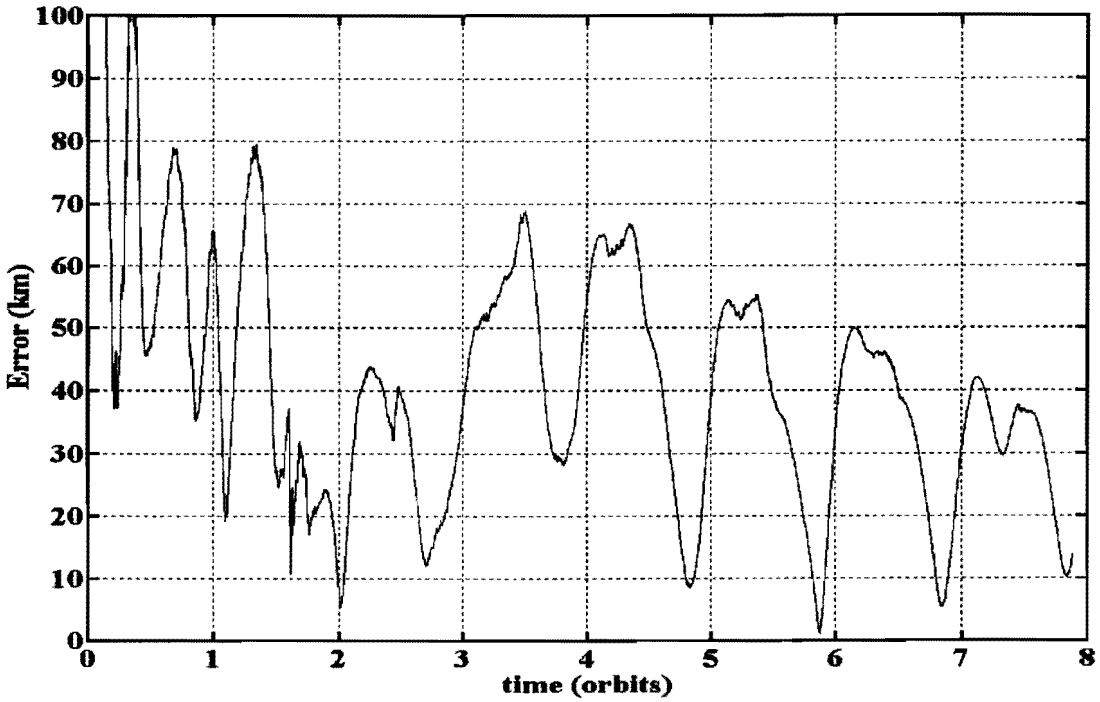

Figure 5. ERBS RSS Position Error, Expanded Vertical Axis

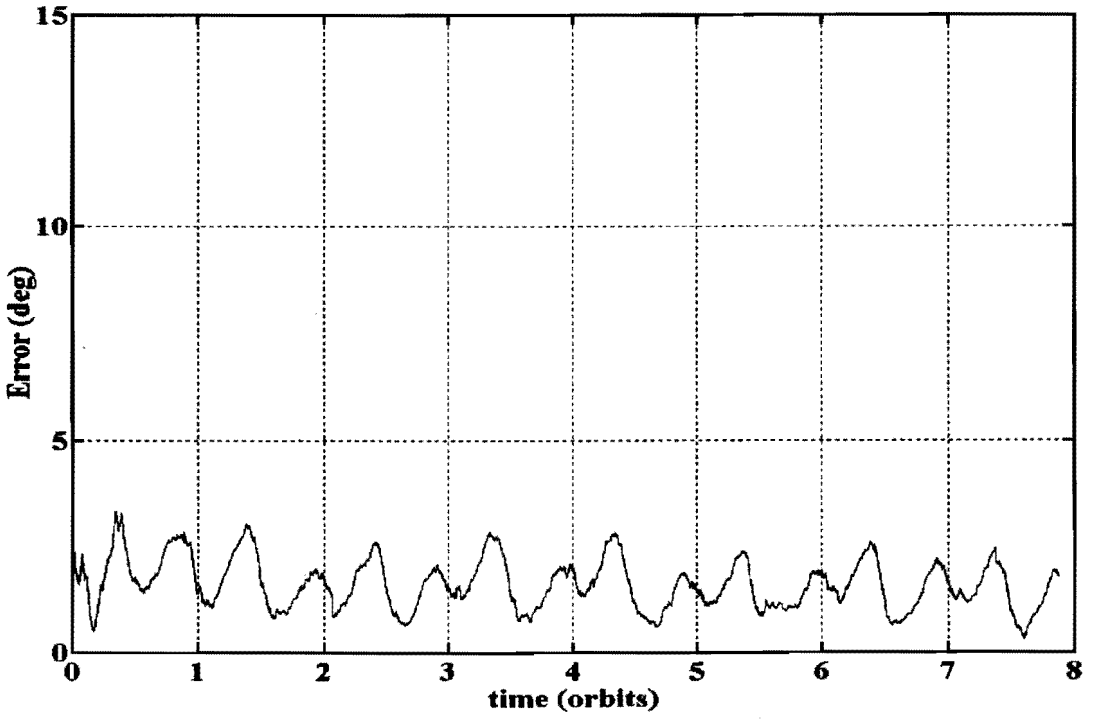

Figure 6. ERBS RSS Attitude Error

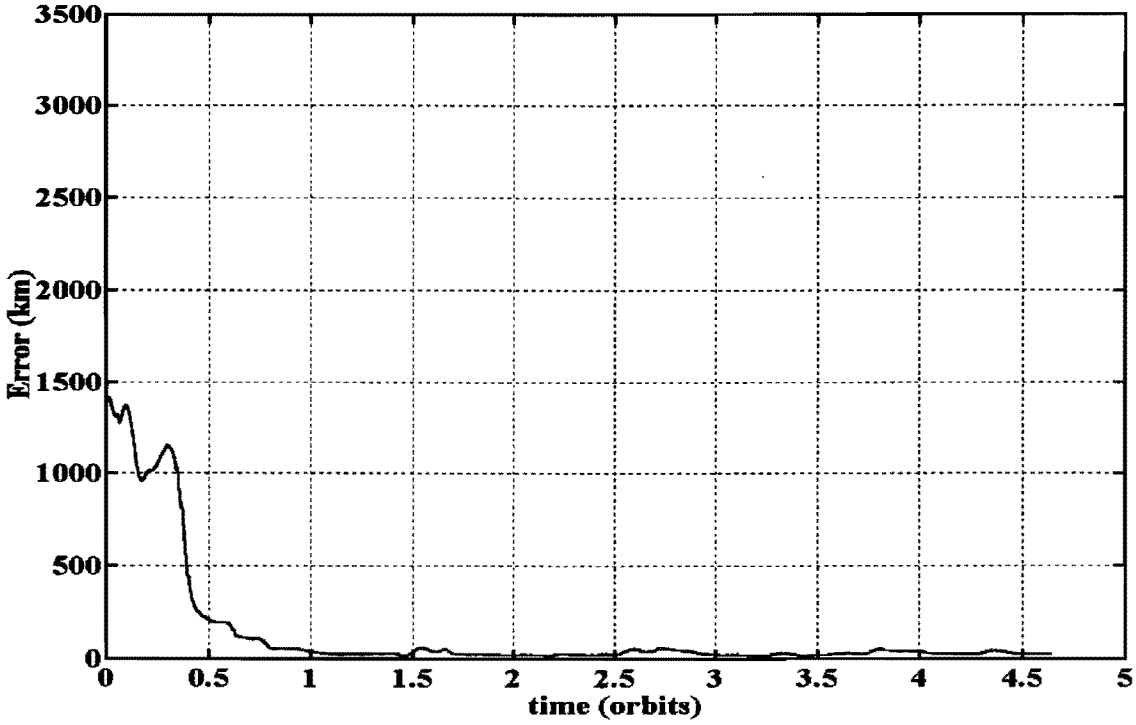

Figure 7. CGRO RSS Position Error

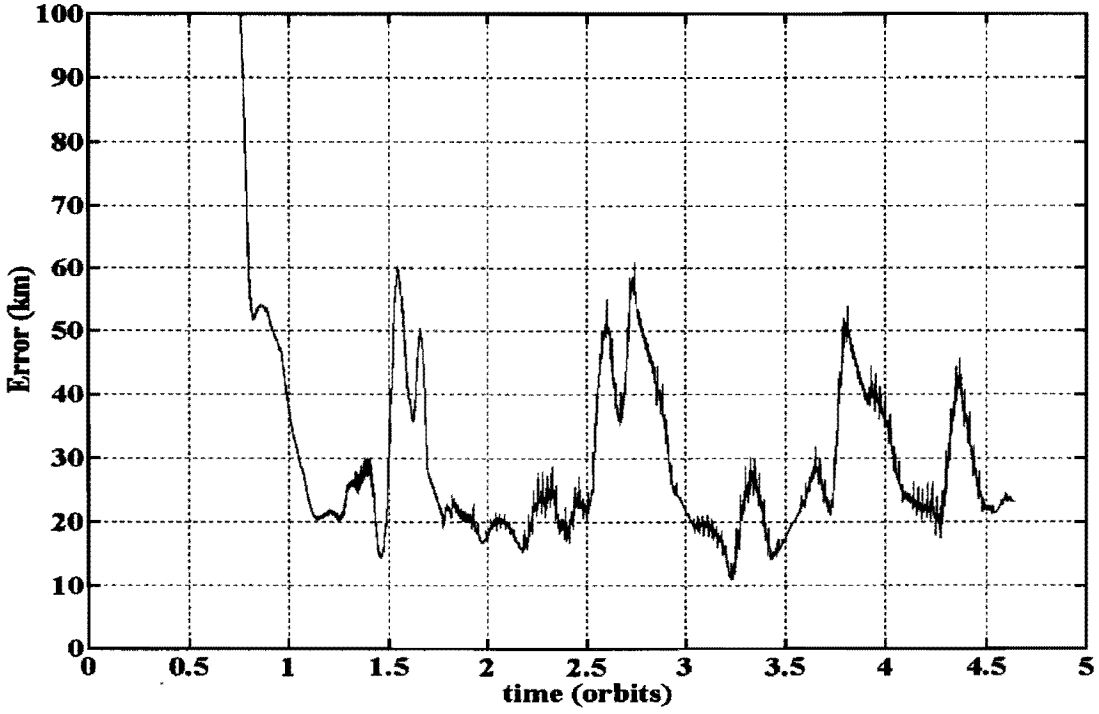

Figure 8. CGRO RSS Position Error, Expanded Vertical Axis

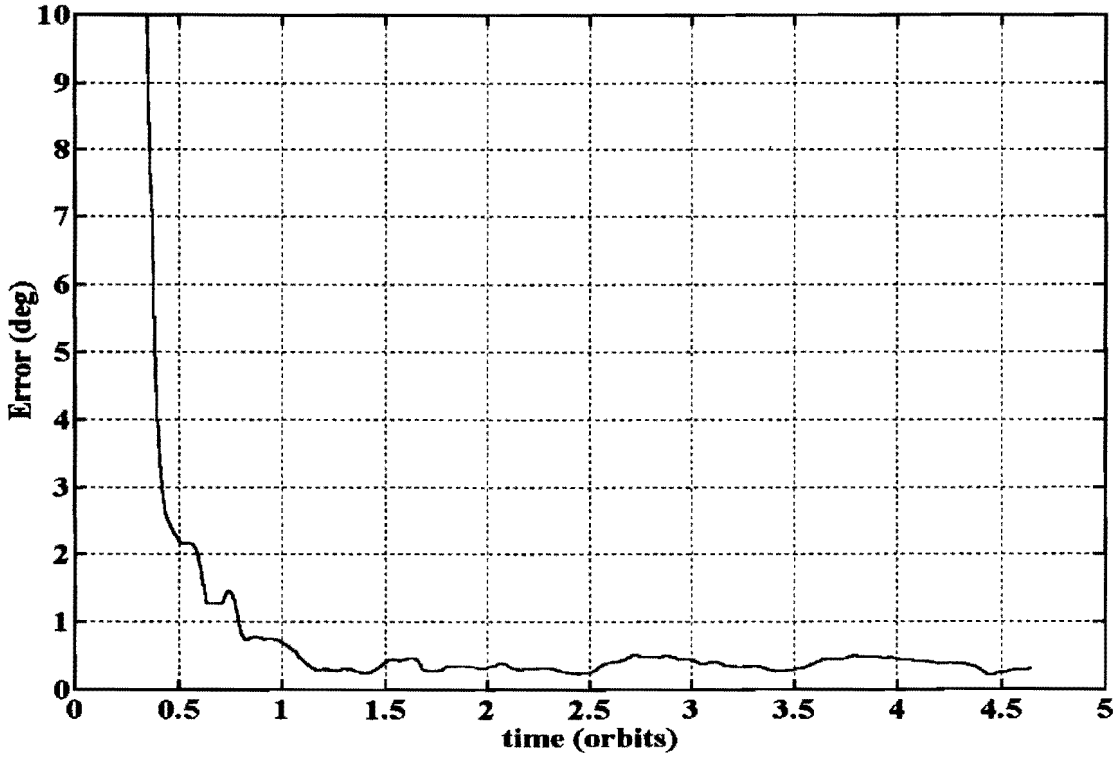

Figure 9. CGRO RSS Attitude Error, Expanded Vertical Axis

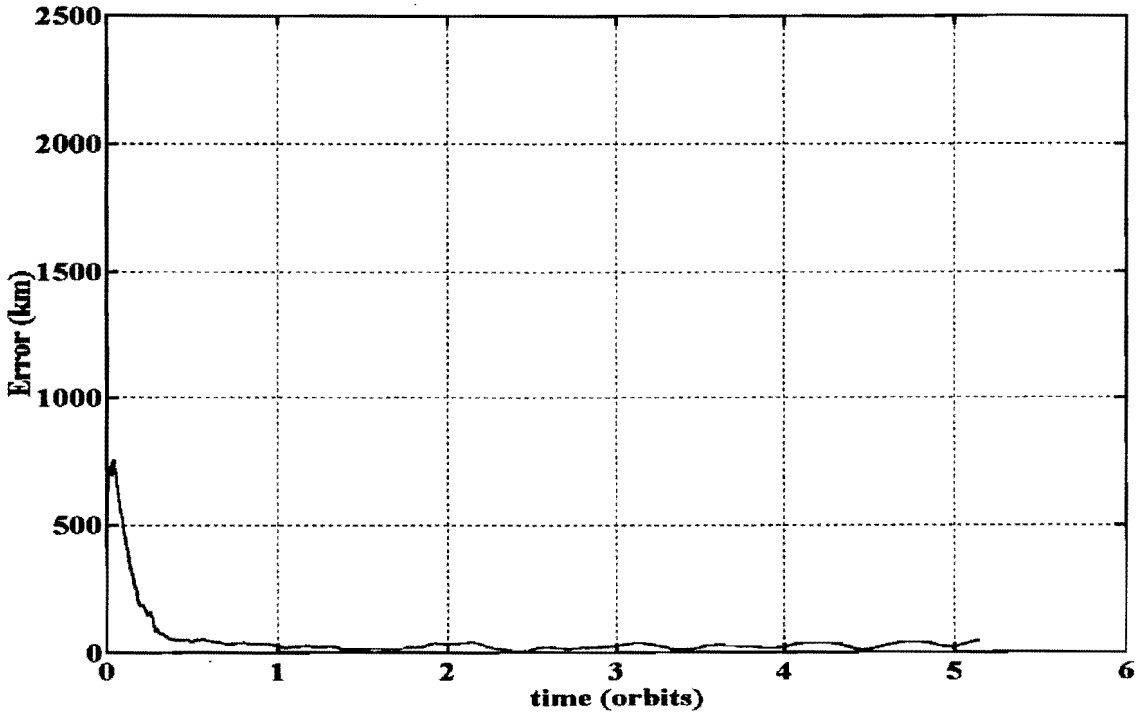

Figure 10. TOMS RSS Position Error

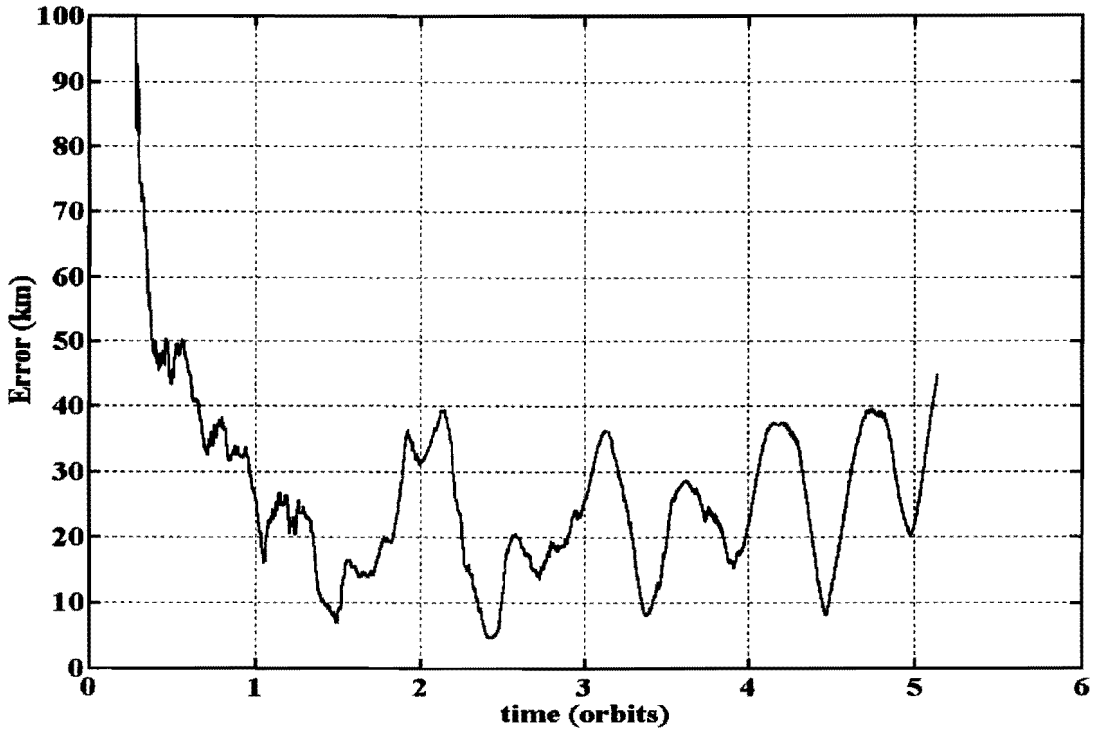

Figure 11. TOMS RSS Position Error, Expanded Vertical Axis

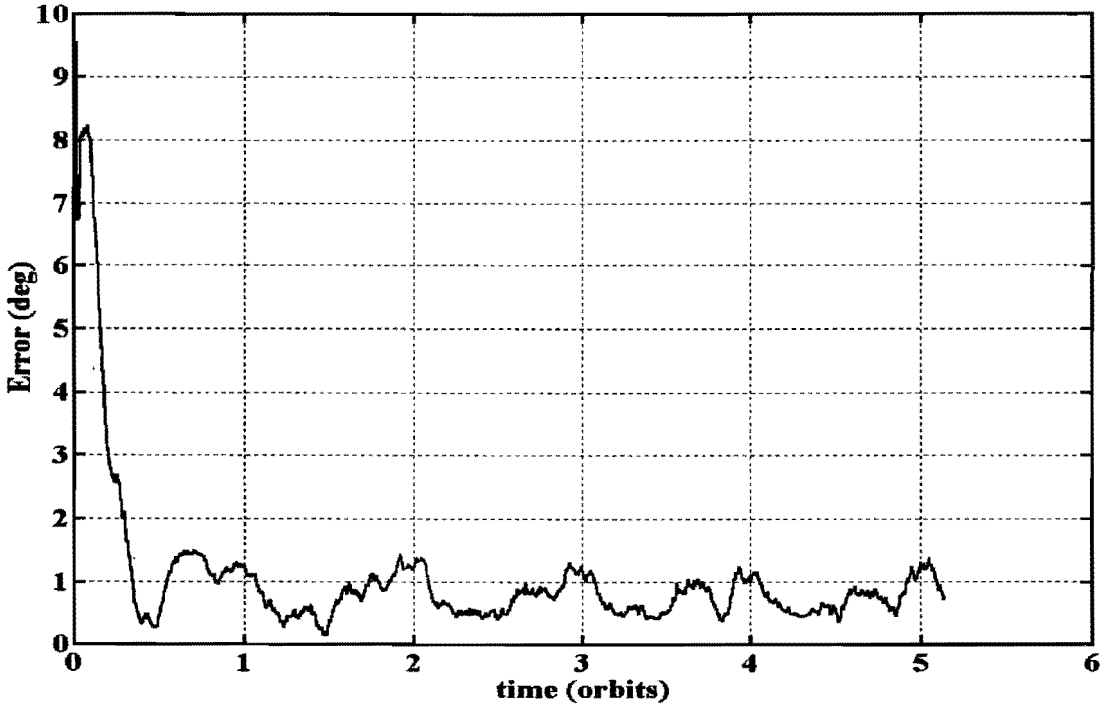

Figure 12. TOMS RSS Attitude Error, Expanded Vertical Axis

convergence and higher accuracy achieved with CGRO. RXTE required more time to converge, with good final results in position. The RXTE magnetometer data contains unknown disturbances that were not calibrated and contribute to the errors in attitude.

Additional CGRO, TOMS, and ERBS data, and more extensive tuning, could probably reduce the final estimates for each. Longer data spans would allow for studies of the steady state behavior of these three. RXTE, which had the longest data span, showed some deviations after the initial convergence due possibly to attitude maneuvers.

References

1. Deutschmann, J. and Bar-Itzhack, I., "Attitude and Trajectory Estimation Using Earth Magnetic Field Data", Paper No. AIAA-96-3631, presented at AIAA/AAS Astrodynamics Conference, San Diego, CA, July 29-31, 1996.

2. Shorshi, G. , and Bar-Itzhack, I., "Satellite Autonomous Navigation Based on Magnetic Field Measurements", Journal of Guidance, Control, and Dynamics, Vol. 18, No. 4 July-August, 1995, pp. 843-850.

3. Ketchum, E., "Autonomous Spacecraft Orbit Determination Using the Magnetic Field and Attitude Information", Paper No. AAS 96-005, presented at 19th Annual AAS Guidance and Control Conference, Breckenridge, Colorado, February 1996.

4. Psiaki, M., "Autonomous Orbit and Magnetic Field Determination Using Magnetometer and Star Sensor Data", Journal of Guidance, Control, and Dynamics, Vol. 18, No. 3, May-June 1995, pp. 584-592.

5. Challa, M., Natanson, G., Deutschmann, J., and Galal, K., "A PC-Based Magnetometer-Only Attitude and Rate Determination System for Gyroless Spacecraft", Paper No. 07, presented at the GSFC FDD Flight Mechanics/Estimation Theory Symposium 1995, NASA GSFC, Greenbelt, Maryland, May 16-18, 1995.

6. Martel, F., Pal, P., and Psiaki, M., "Three-Axis Attitude Determination via Kalman Filtering of Magnetometer Data", presented at the GSFC FDD Flight Mechanics/Estimation Theory Symposium 1988, NASA GSFC, Greenbelt, Maryland, May 10-11, 1988.

7. Hashmall, J., Liu, K., and Rokni, M., "Accurate Spacecraft Attitudes from Magnetometer Data", Paper No. MS95/007, presented at CNES Int'l Symposium on Space Dynamics, Toulouse, France, June 19-23, 1995.

8. Deutschmann, J. Bar-Itzhack, I., and Rokni, M., "Comparison and Testing of Extended Kalman Filters for Attitude Estimation of the Earth Radiation Budget Satellite", presented at the GSFC FDD Flight Mechanics/Estimation Theory Symposium 1990, NASA GSFC, Greenbelt, Maryland, May 22-24, 1990.

9. Kaplan, M.H., *Modern Spacecraft Dynamics & Control*, John Wiley & Sons, New York, 1976.

10. Wertz, James, R., *Spacecraft Attitude Determination and Control*, D. Reidel Publishing Company, Dordrecht, Holland, 1984.

11. Shorshi, G. and Bar-Itzhack, I., "Satellite Autonomous Navigation Based on Magnetic Field Measurements", TAE No. 714, Technion-Israel Institute of Tech., Haifa, Israel, April 1994.

Appendix A. Derivation of the Measurement Matrix

The magnetic field vector can be resolved in the magnetic spherical coordinates, as shown in Figure A.1, as $B^T_F = [B_r, B_{\theta B}, B_{\phi B}]$.

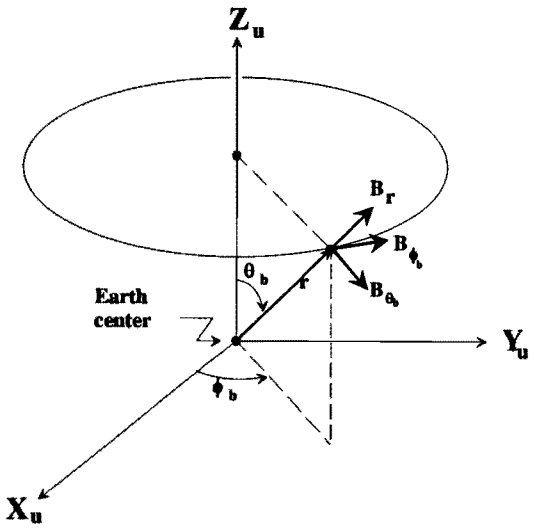

Figure A.1. Definition of the magnetic spherical coordinates

The magnetic field at the spacecraft location, computed using the IGRF magnetic field model and the estimated position, can be written as

$$\underline{\hat{Y}} = \hat{D}_b^I \hat{D}_I^F \underline{\hat{B}}_F + \underline{n}' \qquad (A.1)$$

and the measured magnetic field vector, as measured by the magnetometer can be written as

$$\underline{Y}_m = D_b^I D_I^F \underline{B}_F + \underline{n}_m \qquad (A.2)$$

where

D^I_b = the transformation from inertial to body coordinates
D^F_I = the transformation from magnetic spherical to inertial coordinates
$\underline{n}'$ = the magnetic field model error
$\underline{n}_m$ = the magnetometer measurement error

The effective measurement, $\underline{z}$, is defined as follows

$$\underline{z} = \underline{Y}_m - \underline{\hat{Y}} = D_b^I D_I^F \underline{B}_F + \underline{n}_m - \hat{D}_b^I \hat{D}_I^F \underline{\hat{B}}_F - \underline{n}' \qquad (A.3)$$

Rewriting the transformation of $\underline{\hat{B}}_F$ as

$$\hat{D}_b^I \hat{D}_I^F \underline{\hat{B}}_F = D_b^I D_I^F \underline{B}_F + \Delta(D_b^I D_I^F \underline{B}_F) \qquad (A.4)$$

and

$$\underline{n} = \underline{n}_m - \underline{n}' \qquad (A.5)$$

This leads to

$$\underline{z} = \Delta(D_b^I D_I^F \underline{B}_F) + \underline{n} \qquad (A.6)$$

where

$$\Delta(D_b^I D_I^F \underline{B}_F) = \Delta D_b^I (D_I^F \underline{B}_F) + D_b^I \Delta(D_I^F \underline{B}_F) \qquad (A.7)$$

The second term on the right hand side of equation (A.7) is the derivation of the measurement matrix for the orbital states given in Reference 11. The expansion of the first term leads to the measurement matrix for the attitude states. Rewriting that term as

$$\Delta D_b^I (D_I^F \underline{B}_F) = \Delta D_b^I \underline{B}_I \qquad (A.8)$$

where
$\underline{B}_I$ = the computed magnetic field vector inertial coordinates

The error in the transformation can be defined as the difference between the true body coordinates and an intermediate coordinate system, referred to as the computed body coordinate system. The matrix that is computed is $\hat{D}_b^I$, which is equivalent to a transformation to the computed body coordinate system, which can be written as

$$\hat{D}_b^I = D_c^I = D_c^b D_b^I \qquad (A.9)$$

so

$$\Delta D_b^I = D_c^b D_b^I - D_b^I \qquad (A.10)$$

where D_b^I is the true transformation from inertial to body coordinates. For small attitude error we can assume that the matrix D_c^b is composed of small angles, thus

$$D_c^b = I - \begin{bmatrix} 0 & -\psi & \varphi \\ \psi & 0 & -\phi \\ -\varphi & \phi & 0 \end{bmatrix} = I - [\underline{\alpha}\, x] \qquad (A.11)$$

therefore from equation (A.11)

$$\Delta D_b^I = I - [\underline{\alpha}\, x]\, D_b^I - D_b^I = -[\underline{\alpha}\, x] D_b^I \qquad (A.12)$$

Substituting equation (A.13) into the first term on the right-hand side of equation (A.7) yields

$$\Delta D_b^I (D_I^R \underline{B}_F) = -[\underline{\alpha}\, x] D_b^I \cdot \underline{B}_I = -[\underline{\alpha}\, x]\underline{B}_b = [\underline{B}_b\, x]\underline{\alpha} \qquad (A.13)$$

Substituting equation (A.13) into equation (A.6) along with the measurement matrix for the orbital states, gives

$$\underline{z} = [\underline{B}_b\, x]\underline{\alpha} + H_o \underline{x}_o + \underline{n} = [H_o \;\; [\underline{B}_b\, x]]\underline{x} + \underline{n} \qquad (A.14)$$

where H_o is the measurement matrix for the orbital states, $\underline{x}_o$, and $\underline{x}$ is composed of both the orbital states and the small angular errors in the attitude, $\underline{\alpha}$. Since $\underline{B}_b$ is not known, the magnetic field vector measured by the magnetometer is used instead. The combined measurement matrix is then given as

$$H = [H_o \;\; [B_b\, x]] = [H_o \;\; H_a]$$

Appendix B. Dynamics Equations

The propagation of the state is performed numerically using a Runge-Kutta integration. The differential equations for each of the orbital elements of the state vector $\underline{X}$, including the drag coefficient are given as[9]

$$\dot{a} = \frac{2a}{r}(2a - r)\frac{f_t}{V} \qquad (B.1)$$

$$\dot{e} = \frac{2f_t}{V}(\cos\theta + e) + \frac{f_n}{V}\frac{r}{a}\sin\theta \qquad (B.2)$$

$$\dot{i} = \frac{r f_h}{h}\cos\theta^* \qquad (B.3)$$

$$\dot{\Omega} = \frac{r f_h}{h \sin i}\sin\theta^* \qquad (B.4)$$

$$\dot{\omega} = \frac{1}{e}\left[\frac{2f_t}{V}\sin\theta - \frac{f_n}{V}\left(2e + \frac{r}{a}\cos\theta\right)\right] - \dot{\Omega}\cos i \qquad (B.5)$$

$$\dot{\theta} = \frac{h}{r^2} - \dot{\Omega}\cos i - \dot{\omega} \qquad (B.6)$$

$$\dot{C}_d = 0 \qquad (B.7)$$

where:

$[f_t, f_n, f_h]$ = along-track, radial, and cross track perturbing accelerations due to both drag effects and J_2

$$\theta^* = \omega + \theta$$

$$h = \sqrt{\mu_E a(1 - e^2)}$$

$$r = \frac{a(1 - e^2)}{1 + e\cos\theta}$$

$$V = \sqrt{2\mu_E\left(\frac{1}{r} - \frac{1}{2a}\right)}$$

μ_E = earth gravitation constant

The differential equation governing the dynamics of the attitude quaternion is given by

$$\dot{q} = \frac{1}{2}\Theta q \qquad (B.8)$$

where Θ is a 4x4 skew-symmetric matrix containing the elements of the spacecraft rate vector as measured by the gyros[10].